RSC Advances

PAPER

View Article Online
View Journal | View Issue

Cite this: *RSC Adv.*, 2023, **13**, 16828

Chalcogen-substituted carbenes: a density functional study of structure, stability, and donor ability†

Jamie S. Ritch

Received 18th May 2023
Accepted 26th May 2023

DOI: 10.1039/d3ra03324d

rsc.li/rsc-advances

Chalcogen-substituted carbenes are examined computationally using density functional theory. Several approaches are used to assess the stability and reactivity of chalcogenazol-2-ylidene carbenes (NEHCs; E = O, S, Se, Te). The known unsaturated species 1,3-dimethylimidazol-2-ylidene is studied at the same level of theory as the NEHC molecules, as a reference. Electronic structures, stability towards dimerization, and ligand properties are discussed. The results highlight the NEHCs as potentially valuable ancillary ligands for stabilizing low-valent metals or paramagnetic main group molecules. A simple, effective computational method for evaluating σ donor ability and π acidity of carbenes is presented.

Introduction

N-heterocyclic carbenes (NHCs) are popular spectator ligands due to their modularity, strong σ-donor strength, and in some cases π-acidity.[1] Carbenes featuring heteroatoms other than nitrogen have been of interest since the early days of stable carbene research, including the report of a persistent (phosphino)(silyl)carbene in 1989.[2] In 1997, a benzoxazolyl metal complex was reported,[3] and a thiazol-2-ylidene and its dimer was disclosed.[4] More recently, mesoionic carbenes (MICs, 2001)[5–7] and cyclic (alkyl)(amino) carbenes (CAACs, 2005)[8–10] have yielded examples with unsaturated and saturated carbon centres replacing a nitrogen atom, respectively. These variations on the NHC framework provide ligands with differing substitution patterns and electronic properties (Scheme 1).

For chalcogen-substituted carbenes in particular, thioazol-2-ylidenes (NSHCs) can be prepared using numerous routes,[11–13] and have seen significant use as organocatalysts for transformations such as 1,2 and 1,4 conjugate addition reactions,[14,15] though their coordination chemistry is underexplored.[16] By contrast, NOHCs have only been made using post-coordination ligand modifications of isocyanides,[3] while NSeHC and NTeHCs remain unreported. Given the drastically different electronic properties of the heavier group 16 elements selenium and tellurium compared to lighter congeners, these are potentially valuable synthetic targets with unique chemical properties. Furthermore, NEHC dimerization to give electron-rich alkenes is of interest, as dimer molecules of this type are possible electron donors in conductive organic materials or precursors to stable radical cations. A previous computational study evaluated NEHCs (E = O, S, Se) and proposed NOHC and NSeHC derivatives may show reasonable thermodynamic stability,[17] though there has been no comprehensive evaluation of NEHC (E = O, S, Se, Te) stability, both kinetic and thermodynamic, and their properties for thus far.

There have been many experimental and theoretical studies aimed at quantifying salient properties and finding useful descriptors of NHCs, including donor ability by Tolman electronic parameters (TEPs)[18,19] and ^{77}Se NMR of selenourea derivatives,[20,21] steric encumbrance *via* percent buried volume,[22] and stability and reactivity by calculation of singlet-triplet gaps[23,24] and dimerization energy.[25] The carbene dimerization mechanism has also been modeled computationally,[26–28] and energies of isodesmic reactions between carbenes and methane have been correlated to the carbene dimerization energies.[29]

In this contribution the properties of *N*-methylchalcogenazol-2-ylidene (NEHC; E = O, S, Se, Te) ligands are examined computationally, highlighting their expected properties and possible applications. The electronic structures, stability towards dimerization, and ligand properties of the NEHCs are probed using density functional theory. This is done in comparison to the experimentally known and structurally similar NHC analogue *N*,*N*′-dimethylimidazol-2-ylidene (Me_2im). Me_2im is stable in THF

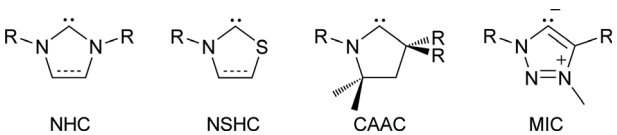

Scheme 1 Structures of common carbenes.

Department of Chemistry, The University of Winnipeg, 515 Portage Avenue, Winnipeg, MB, R3B 2E9, Canada. E-mail: j.ritch@uwinnipeg.ca; Fax: +1-204-774-2401; Tel: +1-204-786-9730

† Electronic supplementary information (ESI) available: Atomic coordinates and energies of all optimized structures (.xyz format). See DOI: https://doi.org/10.1039/d3ra03324d

solution for several days and thus provides a suitable reference for molecules which may be experimentally accessible.

Results and discussion

Ligand geometry and electronic properties

Optimized gas-phase geometries of the five carbenes (ωB97X-D/def2-TZVP) are depicted in Fig. 1. As the MeN group is replaced with increasingly larger chalcogen atoms the obvious effect is distortion of the ring as the carbon–chalcogen bond distances elongate and the C–E–C bond angle contracts. The MeN=C distance also shortens from 1.357 Å in the chalcogenated structures, consistent with increased π donation from the nitrogen lone pair to the divalent carbon atom outcompeting π donation from the chalcogen atom.

The contribution of resonance structures A and B was estimated by Natural Bond Order (NBO) analysis and used to assess the π donor capability of the various groups adjacent to the divalent carbon atom in these structures (Fig. 2), according to the amount of contribution from structure B. This yielded the trend N > S > O > Se > Te. That is, the larger chalcogen atoms are generally poorer at π donation, as would be expected. The greater π donor ability of sulfur *versus* oxygen reflects the very high electronegativity of oxygen. The qualitative trend in π donation was verified by examining the intramolecular donor–acceptor interaction strengths for $n(E) \rightarrow \pi^*(C{=}N)$ (kJ mol^{-1}): 376 (N); 278 (S); 260 (O); 217 (Se); 167 (Te). The differing electron distribution of the NEHCs is also reflected in the natural atomic charges of the N–C–E fragment (Table 1). The carbene C atom in Me_2im is roughly neutral in charge, with flanking negatively charged N atoms. For the NEHCs, the single nitrogen atom retains about the same negative charge as in Me_2im, while the chalcogen atom and carbon atom change significantly. In the NOHC the carbon becomes positively charged with a negative O atom, while for S, Se, and Te the charges are reversed with a negative C atom and positively charged chalcogen centres.

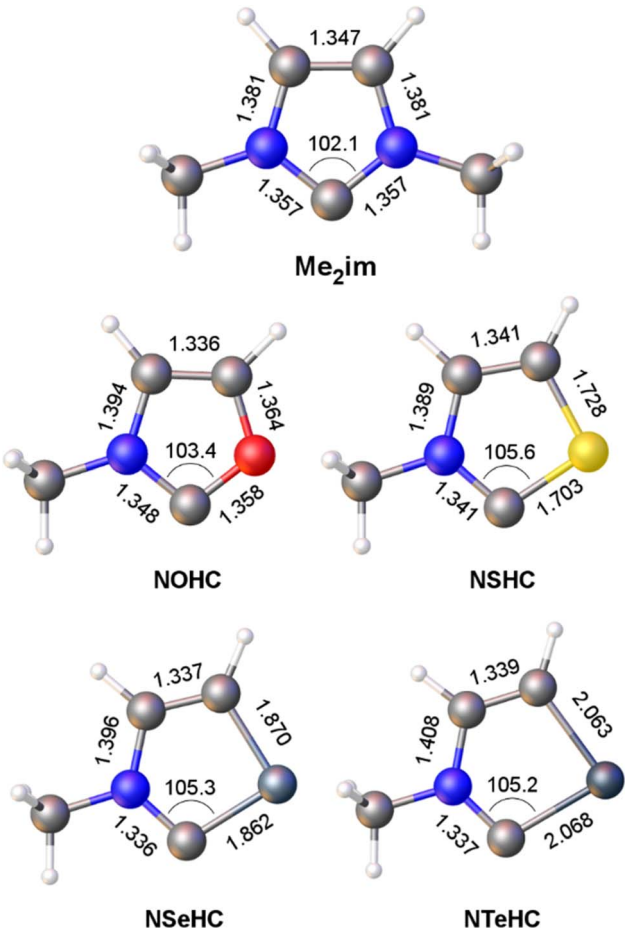

Fig. 1 Calculated bond lengths (Å) and angles (°) for the heterocyclic ligands Me_2im and NEHC (E = O, S, Se, Te).

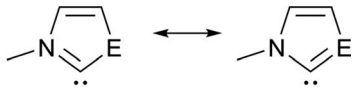

A B

E	%	%
MeN	50	50
O	59	41
S	54	46
Se	57	43
Te	60	40

Fig. 2 Resonance contributors of Me_2im (E = NMe) and NEHC (E = O, S, Se, Te).

Table 1 Natural charges on N–C–E atoms of carbenes

Carbene	C	N	E
Me_2im	+0.07	−0.38	−0.38
NOHC	+0.22	−0.41	−0.42
NSHC	−0.22	−0.38	+0.41
NSeHC	−0.21	−0.40	+0.46
NTeHC	−0.26	−0.42	+0.60

The frontier orbitals of the optimized ligands are depicted in Fig. 3. As the NMe group is replaced with progressively less electronegative chalcogen atoms, the LUMO energy drops steadily. The LUMOs of the chalcogenated rings also have significant contributions from the divalent carbon π-symmetric p orbital, which is absent in Me_2im. The HOMOs of the chalcogenated rings still have the σ-symmetric p orbital on the divalent carbon atom as the main contributor, but increased contributions from the chalcogen centre are seen moving from E = O to E = Te, raising the HOMO energies.

Energies of excitation are listed in Table 2. HOMO–LUMO gaps and vertical singlet–triplet gaps were determined from the transition energy to the first singlet and triplet excited states, respectively, using time-dependent DFT (gap energies calculated using LUMO eigenvalues, *i.e.* values shown in Fig. 3, are normally prone to large errors for hybrid meta GGA functionals).[30] Both vertical (E_{ST}(v)) and adiabatic (E_{ST}(a)) singlet–

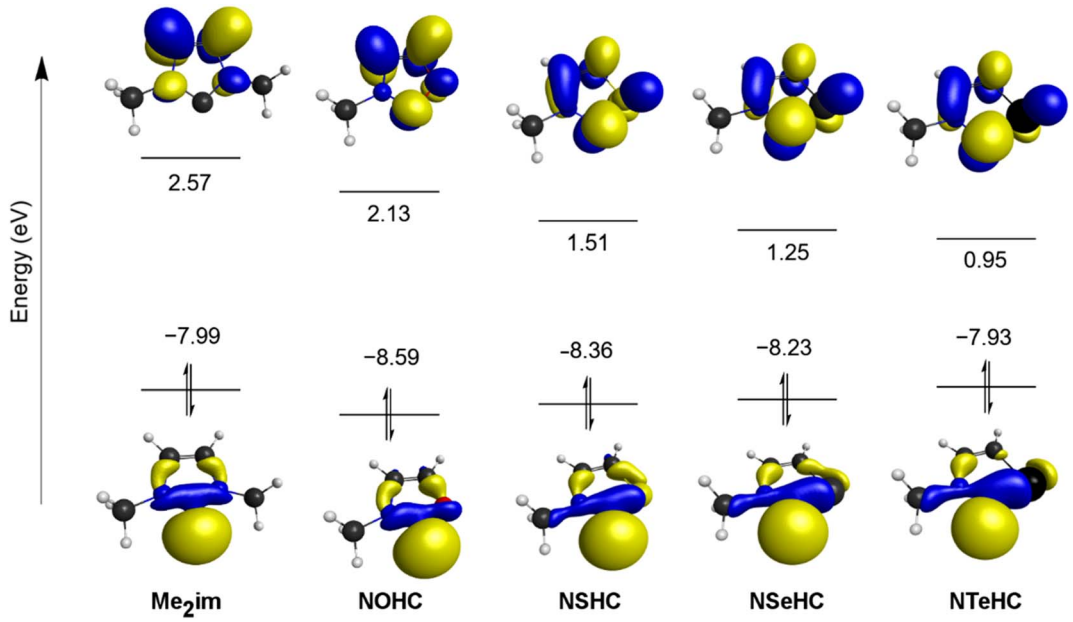

Fig. 3 HOMO and LUMO orbitals for Me_2im and the NEHCs (orbital isosurfaces at 0.05 contour level).

Table 2 Carbene excitation energies (eV) and atomic spin densities (% of total) for triplet states

Compound	HOMO–LUMO gap	E_{ST}(v)	E_{ST}(a)	SD(C)	SD(N)	SD(E)
Me_2im	5.86	4.30	3.75	82.8	5.5	5.5
NOHC	5.61	3.84	3.47	83.9	5.8	5.3
NSHC	4.62	3.34	2.92	79.4	5.5	9.0
NSeHC	4.28	3.07	2.66	78.4	5.4	10.1
NTeHC	3.73	2.67	2.27	75.4	4.7	13.0

triplet gaps are presented. Values for the reference molecule 1,3-dimethylimidazol-2-ylidene (Me_2im)[31] corresponds closely to previously-reported values using B3LYP/aug-cc-PVTZ (the HOMO–LUMO gap, E_{ST}(v) and E_{ST}(a) values differ by <5% from the values in this study),[32] though quite different from results using PBE/TZ2P.[33] The trend in excitation energies predicts the NEHCs should become progressively less thermodynamically stable towards dimerization (*vide infra*), as the singlet-triplet gap of carbenes has shown to be inversely correlated with the dimer C=C bond strength.[23]

Spin density (SD) analysis for the optimized triplet states of the compounds revealed >93% of the spin resides on three atoms: the carbene carbon, and its two neighbours N and E. The spin density on the chalcogen atom is inversely proportional to the electronegativity for the atoms, peaking at 13% of the total for E = Te. These results raise the possibility that heavy chalcogen containing NEHC ligands are more able to bear unpaired electron density when attached to a paramagnetic Lewis acid, compared to the nitrogen atoms of NHCs (*vide infra*).

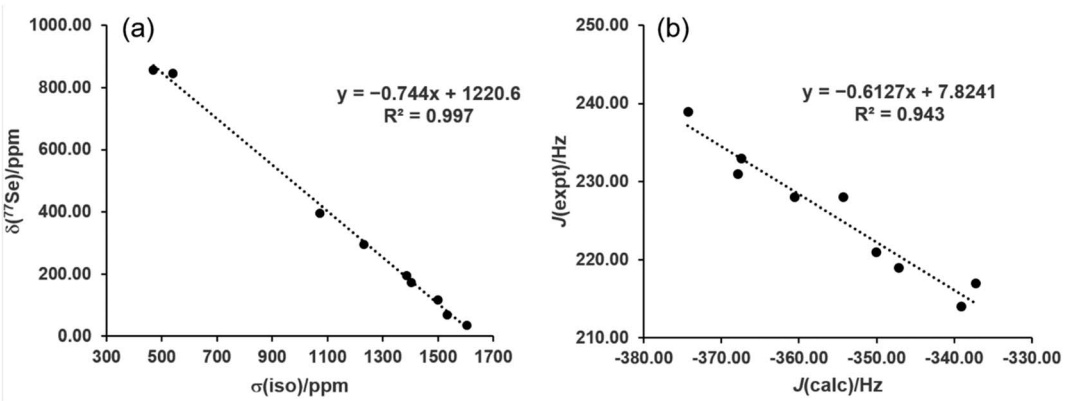

Fig. 4 (a) Experimental ^{77}Se chemical shifts *versus* computed isotropic shielding, and (b) experimental *versus* computed ^{77}Se–^{13}C spin–spin coupling constants.

Donor/acceptor properties of NEHCs

Various descriptors of the electronic properties of NHCs have been proposed. Their σ donor ability has been correlated with computed HOMO eigenvalues and N–C–N bond angles.[32] Spectroscopic measures of NHC derivatives including the $\nu_{CO}(A_1)$ mode of $[Ni(CO)_3L]$ (Tolman Electronic Parameter, TEP),[34] thought to reflect both σ-donor and π-acceptor properties, and the $\delta(^{13}C_{carbene})$ of 1,3-diisopropylbenzimidazolin-2-ylidene ($^iPr_2$-bimy) in *trans*-$[PdBr_2L(^iPr_2bimy)]$ (Huynh Electronic Parameter, HEP) which measures primarily σ-donor behaviour.[35] The $^1J(^{13}C–^1H)$ value of protonated carbene precursors has been correlated to σ donor ability of the carbene.[20,36] Bertrand *et al.* have disclosed the use of $\delta(^{31}P)$ of NHC-phosphinidene adducts as a gauge of π-acidity, while Ganter *et al.* reported using the $\delta(^{77}Se)$ of easily-prepared NHC = Se derivatives to ascertain π-acidity of the parent carbene,[21] and the $^1J(^{77}Se–^{13}C)$ to measure σ-donor ability. Computational work later showed that isotropic shielding of the Se atoms calculated at the BP86/TZ2P level correlated well with the experimental δ_{Se} values.[37]

In the present study, a series of calculations was performed to determine if both the ^{77}Se chemical shift values and $^1J(^{77}Se–^{13}C)$ coupling constants of selenoureas could be replicated using rapid and readily-available electronic structure methods. In this way a predictive model could be developed and applied to the NEHCs under study, and provided for use by other researchers. A set of nine reported selenoureas were modeled, as the experimental ^{77}Se chemical shifts (in acetone-d_6) and coupling constants (in $CDCl_3$) for each were determined under the same experimental conditions.[20]

While the range-separated hybrid functional ωB97X-D is used in this study for reaction energetics, the computationally less expensive pure GGA functional PBE was investigated for NMR property calculations. The nine gas-phase reference structures were optimized at the PBE/def2-TZVP level and the isotropic shielding at Se as well as the (C,Se) spin–spin coupling constants were calculated for these structures. The zeroth-order relativistic approximation (ZORA) was used along with the appropriate relativistically-contracted basis set for the property calculations. Plotting the shielding values (σ_{iso}) *versus* the measured chemical shifts (δ_{Se}) and performing linear regression yielded excellent agreement ($R^2 = 0.997$) with the equation $\delta_{Se} = -0.744\sigma_{iso} + 1220.6$ (Fig. 4a). The values predicted from this equation give a mean absolute error (MAE) of 15.6 ppm, and yielded the correct ordering of compounds from low to high predicted chemical shift. This method thus is recommended for ^{77}Se shift calculations of selenoureas as it has a low computational cost and high accuracy. It is also convenient to evaluate both σ donor ability and π acidity of a carbene from NMR calculations of a single optimized structure. Given the large structural variety of the nine reference carbenes the model is very promising, though additional carbene experimental data would further verify its utility.

The same level of theory, when used to calculate the $^1J(^{77}Se–^{13}C)$ spin–spin coupling constants, gave very good linear fitting ($R^2 = 0.943$, MAE = 1.7 Hz) to experimental values with the equation $J_{Se,C} = -0.6127J_{calc} + 7.8241$ (Fig. 4b). The overall trend in values is reproduced, though due to the relatively small spread between the nine experimental *J* values the predicted ordering was not always correct for values within a few Hz of each other.

Table 3 Calculated NMR properties for NEHCs

	^{77}Se (ppm)		$^1J_{Se,C}$ (Hz)	
Carbene	Me	^{t}Bu	Me	^{t}Bu
Me_2im	68.39	—	233.83	—
NOHC	141.85	191.67	253.15	253.17
NSHC	408.06	445.10	234.94	235.95
NSeHC	506.83	543.62	238.46	240.69
NTeHC	715.76	752.00	234.62	236.64

Applying these new models to the NEHCs and Me_2im yielded predicted ^{77}Se parameters as shown in Table 3. The predicted ordering of σ donor ability is thus: Me_2im > NTeHC > NSHC > NSeHC ≫ NOHC; the π-acidity trend is NTeHC > NSeHC > NSHC > NOHC > Me_2im. Fig. 5 and 6 display the nine experimental δ_{Se} and J_{SeC} values along with the predicted values. The NEHCs under study are thus predicted to be similar to IMes in terms of σ donor ability, though slightly weaker (except for the NOHC which is significantly weaker), while being stronger π-acceptors. Such carbenes are valued for stabilizing low-valent metal complexes and open-shell species.[38] The reported ^{77}Se resonance for a CAAC selone derivative with aromatic *N*-substitution (+492 ppm)[39] indicates a similar π acidity to the NSHC and NSeHC ligands. Since CAACs have found use in preparing low valent d-block complexes[40] and main group radicals,[41] this bodes well for the future use of NEHCs in this manner.

To probe steric effects, the NMR properties of *tert*-butyl substituted NEHC selenoureas have been determined using the new model (Table 3). The predicted ^{77}Se chemical shift values are higher by 50 ppm for the oxygen derivative and *ca.* 37 ppm for the heavier derivatives. The $^1J_{Se–C}$ values are nearly identical for oxygen but higher by 1–2 Hz for the heavier derivatives. Interestingly, this indicates the *tert*-butyl substituted carbenes are, compared to R = Me, slightly more π-acidic and slightly less σ-donating. The seemingly unintuitive result of a less donating when a more electron-releasing alkyl group is present has precedent – Ganter and coworkers[20] revealed that the introduction of one or two carbonyl groups in the backbone of *N*-mesityl-substituted carbenes increased their σ donor ability relative to IMes.

Dimerization

Bulky *N*-substituents generally disfavour the dimerization of NHCs to give electron-rich olefins. In the case of imidazole-2-ylidenes, aromaticity of the five-membered ring also disfavours this process. For instance, the relatively unhindered carbene Me_2im is not known to dimerize but rather decomposes slowly *via* other pathways upon storage at −30 °C.[31] However, some imidazoline-2-ylidenes and benzimidazole-2-ylidenes

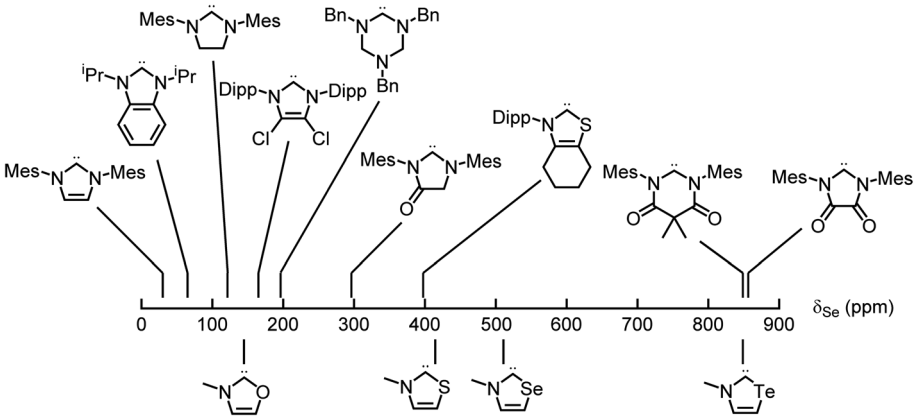

Fig. 5 Experimental (top) and predicted (bottom) ^{77}Se chemical shifts of the selone derivatives of carbenes – π acidity increases to the right.

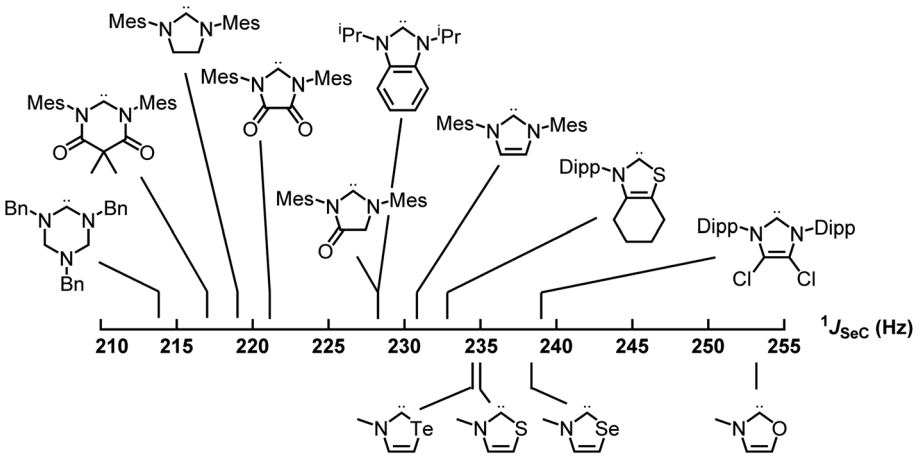

Fig. 6 Experimental (top) and predicted (bottom) ^{77}Se–^{13}C spin–spin coupling constants of the selone derivatives of carbenes – σ donor strength increases to the left.

with smaller substituents and/or less aromatic stabilization, are known to dimerize. The interconversion of NHCs and other cyclic carbenes and their dimer tetraaminoethylene derivatives has been studied experimentally and theoretically. It is generally accepted that a proton-catalyzed pathway operates in most instances as opposed to a direct one-step dimerization, however the latter is possible in some instances.[27,42]

The smaller the singlet-triplet gap, the stronger the C=C bond in the resulting carbene dimer, and hence the more thermodynamically favoured dimerization will be.[23,24] In the context of the chalcogen-substituted NEHC carbenes, given their small singlet–triplet gaps, the direct uncatalyzed dimerization process is possible. Arduengo and coworkers reported a stable thiazolylidene (featuring methylation on the backbone and a Dipp substituent on nitrogen) which formed an *anti*-configuration dimer when catalyzed by the protonated thiazolium salt.[4] In a previous report,[17] dimerization energies for NEHCs (E = O, S, Se) were estimated using a correlation between Δ(E) of an isodesmic reaction of the carbene with methane and the dimerization energy, predicting the dimers are thermodynamically favoured.[29] This approach accounts for only electronic factors, and estimates thermodynamic stability. There have been no previous computational dimerization studies on the entire series of group 16 NEHCs, nor any including both kinetic and thermodynamic aspects of dimerization.

Direct dimerization of NEHCs and Me_2im was examined using DFT, and a set of *t*-butyl-substituted NEHC ligands was also examined to probe the effect of sterics at the nitrogen centres. These *tert*-butyl analogues had computed HOMO–LUMO gaps and vertical triplet excitation energies only slightly lower (by *ca.* 0.5–1.5%) compared to the methyl-substituted carbenes. Thus, their electronic structures are very similar, and significant differences in reaction energetics will be reflective of the effect of increased steric bulk at nitrogen. Both *E*/*Z* stereochemical outcomes were studied for each carbene (Scheme 2). One transition state was located for each reaction, and their structures indicated a non-least-motion pathway for each process. Using the intrinsic reaction coordinate method, dimer structures were located from the transition states and optimized, revealing that all (*Z*)-dimers had *anti*-orientations of the five-membered rings (oriented towards different faces of the

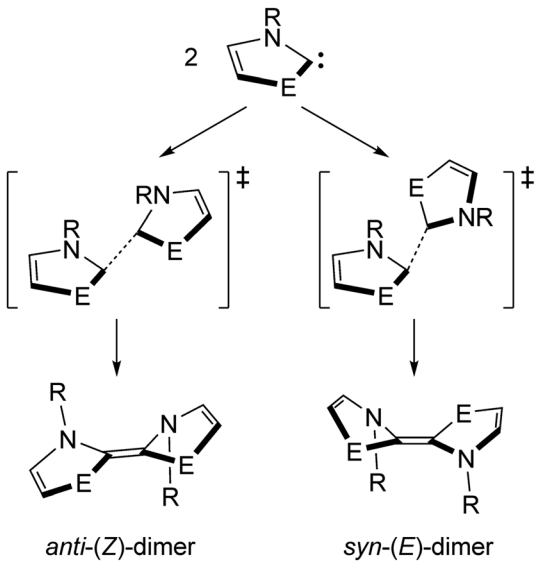

Scheme 2 The *E*/*Z* dimerization of NEHCs.

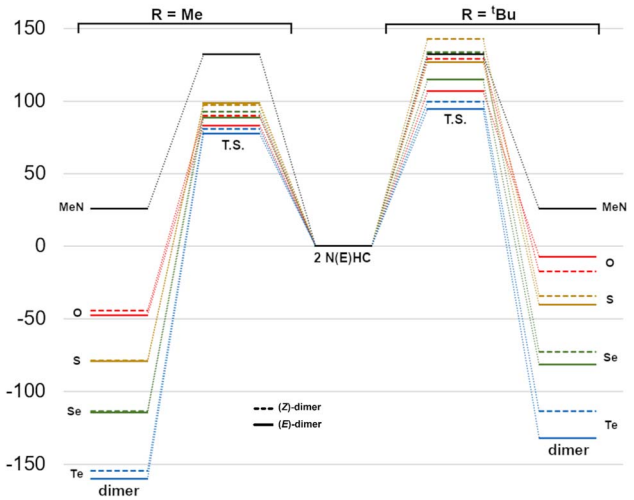

Fig. 7 Reaction Gibbs energy diagram for dimerization (kJ mol^{-1}) of Me_2im and the NEHCs (centre) to give methyl- (left) or *tert*-butyl-substituted dimers (right).

alkene), while the (*E*)-dimers were *syn* (oriented towards the same face of the alkene). One of the studied NEHC dimers has been previously experimentally observed: the sulfur (*E*)-dimer with R = Me was crystallographically characterized by Arduengo and coworkers.[4] Compared to the experimental atomic coordinates, the computed structure was very similar (RMSD of 0.126 Å for atomic coordinates of non-H atoms) indicating the suitability of the computational methodology for structures of this type.

The reaction energetics for the dimerization processes are shown in Fig. 7. For Me_2im, the dimerization is both kinetically and thermodynamically disfavoured ($\Delta G^{\ddagger}$ and ΔG° of +132 and +25.7 kJ mol^{-1}, respectively), consistent with the experimental observation that this carbene does not form a dimer. For NEHCs, the *E* dimerizations had, on average, lower activation barriers by 11 kJ mol^{-1} and more negative reaction Gibbs energies by 6 kJ mol^{-1}. The two exceptions to this were for E = S and R = Me, where the *Z* dimerization had a roughly equivalent barrier to the (*E*) process (1.5 kJ mol^{-1} lower), and for E = O and R = ^{t}Bu, where the (*Z*)-dimer was *ca.* 10 kJ mol^{-1} more stable (*vide infra*). Energetic differences between *E* and *Z* processes were more pronounced for *tert*-butyl-substituted NEHCS and, for a given NEHC, changing from methyl to *tert*-butyl substituents increased the reaction barrier by an average of 30 kJ mol^{-1} and decreased stability of the dimer relative to the monomers by 6 kJ mol^{-1}.

The reaction barriers can be attributed to the energy required to cause electronic reorganization of the carbenes, *i.e.* disruption of π bonding and loss of aromaticity. This is evidenced by pyramidalization of the nitrogen centres and lengthening of the carbene C–N and C–E bonds in the transition states (Table 4). The *tert*-butyl-substituted derivatives require more energy to pyramidalize the nitrogen centres and feature more intra- and intermolecular steric repulsions in the transition state geometries, increasing their activation energies. Whereas for the NEHC dimer products, the interplanar angles between the two five-membered rings are in the narrow range of *ca.* 0°–13° (and 17.4° for the Me_2im dimer), the transition state values vary from *ca.* 0–89°, with the *Z* geometries generally featuring higher angles than *E*.

Table 4 Geometric data for dimerization transition states and dimers

	θ_{TS}		θ_{dimer}		d(C=C)$_{TS}$		d(C=C)$_{dimer}$		
NEHC	Me	^{t}Bu	Me	^{t}Bu	Me	^{t}Bu	Me	^{t}Bu	Conformation
MeN	49.2		17.4		1.79		1.35		*anti*
(*E*)-O	2.8	0	0.2	0	1.94	1.91	1.33	1.34	*anti*
(*Z*)-O	30	50.7	7.9	13.1	1.92	1.93	1.33	1.34	*anti*
(*E*)-S	30.2	49.1	8.7	10.9	2.01	1.94	1.34	1.34	*syn*
(*Z*)-S	63.5	54.4	8.7	9.1	1.96	1.96	1.34	1.35	*anti*
(*E*)-Se	38.1	51.7	9.3	11.3	2.06	2	1.34	1.33	*syn*
(*Z*)-Se	69.9	58.1	9.6	8.8	2	1.99	1.34	1.34	*anti*
(*E*)-Te	89.3	53.7	10.1	11.9	2.14	2.08	1.34	1.33	*syn*
(*Z*)-Te	74.3	82.9	10.4	9.2	2.08	1.96	1.34	1.34	*anti*

The C=C bond length of all the NEHC dimers were in the narrow range of 1.33–1.34 Å, whereas the C···C distance in the transition states varied from 1.91–2.08 Å (and was 1.79 Å for Me_2im dimerization). The methyl-substituted transition states had longer distances by, on average, 0.04 Å. The bending of the five-membered rings out of the plane of the alkene to either *syn* or *anti* configurations was also more pronounced for the bulkier *tert*-butyl derivatives. For the E = O, R = Me dimers the deviation from planarity was only slight, making the (*E*)-dimer higher in energy than (*Z*) due to oxygen···*tert*-butyl group repulsive interactions between the two rings, which are avoided in the other NEHCS due to more substantial ring bending.

Overall, the thermodynamics of dimerization reveal that all methyl-substituted NEHCs have a $\Delta G^{\ddagger}$ ranging from ∼75–100 kJ mol^{-1} and would consequently dimerize at room temperature to give an *E*/*Z* mixture, favouring the (*E*)-dimer in most cases. Dimerization would be rapid, except for the sulfur derivative which has barriers near 100 kJ mol^{-1}. Substitution with *tert*-butyl groups has a stabilizing effect on the NEHCs and is predicted to yield kinetically stable carbenes in all cases (barriers > ∼95 kJ mol^{-1}). Lower energy proton-catalyzed pathways are likely, and so experimentally prepared NEHCs should be handled carefully under aprotic conditions. The dimers are thermodynamically favoured in all cases, and none of the NEHC dimers studied have thermally accessible monomers at reasonable temperature *via* the studied pathway. These NEHC dimers may in and of themselves be intriguing synthetic targets, due to their possible use as organic electron donors akin to the tetrathiafulvalenes.[43]

Stabilization of main group radicals

Given the predicted high π-accepting properties of NEHCs, they may have utility to stabilize paramagnetic species *via* spin delocalization onto the carbene ligand. To probe this possibility, the ability of NEHCs to stabilize a main-group radical system was also investigated. The species [NHC–BH_2]$^{\bullet}$ are known to be generated by photolysis in the presence of a radical initiator and are observable by EPR spectroscopy,[44] and find utility in promoting radical reactions and polymerization processes.[45] While organosubstituted NHC–BR_2 analogues can be rendered persistent,[46] the BH_2 analogues rapidly decompose in the absence of steric protection and/or increased delocalization. While NEHCs have only one nitrogen substituent for steric protection *versus* two in NHCs, the chalcogen atom is expected to have a significant effect on electronic stabilization of radicals. To model the influence of chalcogen substitution on this class of compound, energetics were computed using Me-substituted NEHCs and Me_2im for boryl radical formation, and dimerization of the boryl radical to a diborane, which has been observed experimentally for monosubstituted systems NHC–B(R)H,[44] and during the reduction of NHC–BBr_3.[47] The former process was modelled as the hydrogen atom abstraction from the borane adducts of the ligands by *tert*-butoxide radical (eqn (1)), while the latter was modelled as the dimerization of two NEHC–$BH_2^{\bullet}$ radicals (eqn (2)).

Table 5 Gibbs energies of reaction for eqn (1) and (2)

Ligand	Me_2im	NOHC	NSHC	NSeHC	NTeHC
$\Delta G^{\circ}_{rxn}(1)$	−104.1	−123.5	−138.2	−145.7	−153.6
$\Delta G^{\circ}_{rxn}(2)^a$	−121.7	−87.7	−61.2	−47.8	−34.2

[a] Where (*E*)- and (*Z*)-dimers are possible, the lowest ΔG of the two reactions is reported (values were within 2–6 kJ mol^{-1} for isomers).

Table 6 Natural spin density (% of total) of NEHC–BH_2 radicals

Ligand	Me_2im	NOHC	NSHC	NSeHC	NTeHC
SD(B)	55.9	48.0	38.8	36.3	33.2
SD(C)	10.9	20.7	20.4	21.8	22.8
SD(N)	15.4	17.3	17.8	17.6	17.4
SD(E)	15.4	12.0	20.5	21.6	23.0

$$NEHC\text{–}BH_3 + {}^{t}BuO^{\bullet} \rightarrow [NEHC\text{–}BH_2]^{\bullet} + {}^{t}BuOH \quad (1)$$

$$2[NEHC\text{–}BH_2]^{\bullet} \rightarrow [(NEHC)BH_2\text{–}BH_2(NEHC)] \quad (2)$$

The Gibbs energy changes (Table 5) for eqn (1) show that hydrogen atom abstraction is more favourable for the chalcogenated NEHC ligands *versus* Me_2im, to an increasing degree as the chalcogen size increases. Natural population analysis was performed to analyze the spin density of the radical products (Table 6). In all cases the spin density on N–C–E atoms and the boron centre comprised >96% of the total spin. As chalcogen size increases, spin density on boron decreases with a concomitant increase at the chalcogen atom, while the sum of the spin densities on the carbene C and N atoms remains essentially the same at *ca.* 38–40%. In the case of Me_2im, over 55% of the spin density resides on the boron atom, whereas for the NEHCs less than half of the spin density is found at the B atom. The tendency of the radicals to dimerize also decreases with increasing chalcogen size, with ΔG° values for the NEHCs ranging from *ca.* −88 to −34 kJ mol^{-1}, *cf.* −122 for Me_2im. The NEHCs are thus feasible candidates for the stabilization of paramagnetic species such as BH_2, particularly for the heavier Se and Te analogues and with a large substituent at nitrogen for additional steric protection.

Conclusions

The first computational study of a full series of chalcogenazol-2-ylidene (NEHC) carbenes indicates they are attractive synthetic targets with a number of potentially useful ligand properties. While more likely to undergo dimerization than NHCs, the species should be useable *in situ*, and stabilization by additional steric protection, or the use of a silver complex as a transfer agent may increase their utility. The simple and rapid computational model for carbene donor properties presented is promising, and warrants validation using experimental data from an expanded library of carbenes. The predicted weaker σ donor and stronger π acceptor properties of NEHCs compared to commonly-used NHCs make them suitable for coordination

to electron-rich metals, or for stabilizing paramagnetic main group species. The NEHC dimers are also valuable targets as possible sources of organic electron donors, organocatalysts, and precursors to stable organic radicals. Experimental studies of possible synthetic routes to NEHCs and their dimers are currently underway.

Experimental section

Computational details

Geometry optimizations were performed with the GAMESS[48] package without symmetry constraints utilizing the ωB97X-D[49] density functional, from starting coordinates calculated at the Hartree–Fock level of theory. This hybrid meta-GGA functional was used as it a generally strong performer for main group thermochemistry.[50] The triple-ζ basis set def2-TZVP[51] was used for all atoms. For tellurium, the core electrons were modelled using an effective core potential (ECP). Closed shell species were modeled using the spin-restricted formalism, while open shell species were modeled with the spin-unrestricted formalism. Hessian calculations were performed to confirm the nature of all stationary points as either local minima or maxima on the potential energy surface, and to obtain thermochemical corrections at standard conditions. Gibbs energies are calculated at 1 atm and 298.15 K. For reaction studies, transition states were evaluated using the intrinsic reaction coordinate (IRC) method to ensure they were connected to the proposed reactants and products. Geometric analyses were performed on transition state geometries using the Olex2 software package.[52] Interplanar angles (θ) are the minimum angles between the normals of the least-squares planes for the five ring atoms on each NEHC fragment, when viewed down the C═C bond.

Natural bond orbital (NBO) calculations, including natural atomic charges and natural atomic spin densities by Natural Population Analysis (NPA), and donor–acceptor interactions using second-order perturbation theory analysis of the Fock matrix, were performed using the program NBO7,[53] as interfaced with Gaussian16,[54] at the same level of theory as the geometry optimizations (ωB97X-D/def2-TZVP).

NMR properties were evaluated with the ORCA[55] package (version 5.0.3) by first optimizing geometries of the selenoureas at the PBE/def2-TZVP level of theory, and then performing NMR shielding and spin–spin coupling calculations including the zeroth-order regular approximation (ZORA)[56] using the PBE[57] functional and relativistically-contracted all-electron basis sets (SARC[58] for tellurium, and ZORA-def2-TZVP as implemented in ORCA for all other elements). The Resolution of Identity approximation for Coulomb integrals (RI-J) was used for ORCA calculations.

Conflicts of interest

There are no conflicts of interest to declare.

Acknowledgements

Financial support from NSERC (Canada) and The University of Winnipeg, as well as computational resources from Digital Research Alliance of Canada, are gratefully acknowledged. Dr Joshua Hollett is thanked for useful discussions.

References

1 M. N. Hopkinson, C. Richter, M. Schedler and F. Glorius, *Nature*, 2014, **510**, 485–496.
2 A. Igau, A. Baceiredo, G. Trinquier and G. Bertrand, *Angew. Chem., Int. Ed. Engl.*, 1989, **28**, 621–622.
3 F. E. Hahn, M. Tamm and T. Lügger, *Angew. Chem., Int. Ed. Engl.*, 1994, **33**, 1356–1359.
4 A. J. Arduengo, J. R. Goerlich and W. J. Marshall, *Liebigs Ann.*, 1997, **1997**, 365–374.
5 S. Gründemann, A. Kovacevic, M. Albrecht, J. W. F. Robert and H. Crabtree, *Chem. Commun.*, 2001, 2274–2275.
6 O. Schuster, L. Yang, H. G. Raubenheimer and M. Albrecht, *Chem. Rev.*, 2009, **109**, 3445–3478.
7 R. H. Crabtree, *Coord. Chem. Rev.*, 2013, **257**, 755–766.
8 V. Lavallo, Y. Canac, C. Präsang, B. Donnadieu and G. Bertrand, *Angew. Chem., Int. Ed.*, 2005, **44**, 5705–5709.
9 M. Soleilhavoup and G. Bertrand, *Acc. Chem. Res.*, 2015, **48**, 256–266.
10 M. Melaimi, R. Jazzar, M. Soleilhavoup and G. Bertrand, *Angew. Chem., Int. Ed.*, 2017, **56**, 10046–10068.
11 R. Lebeuf, K. Hirano and F. Glorius, *Org. Lett.*, 2008, **10**, 4243–4246.
12 I. Piel, M. D. Pawelczyk, K. Hirano, R. Fröhlich and F. Glorius, *Eur. J. Org. Chem.*, 2011, **2011**, 5475–5484.
13 J. F. Binder, A. M. Corrente and C. L. B. Macdonald, *Dalton Trans.*, 2016, **45**, 2138–2147.
14 D. Enders, O. Niemeier and A. Henseler, *Chem. Rev.*, 2007, **107**, 5606–5655.
15 D. M. Flanigan, F. Romanov-Michailidis, N. A. White and T. Rovis, *Chem. Rev.*, 2015, **115**, 9307–9387.
16 J. Zhang, T. Li, X. Li, A. Lv, X. Li, Z. Wang, R. Wang, Y. Ma, R. Fang, R. Szostak and M. Szostak, *Commun. Chem.*, 2022, **5**, 1–11.
17 Z. Kelemen, O. Hollóczki, J. Oláh and L. Nyulászi, *RSC Adv.*, 2013, **3**, 7970–7978.
18 D. G. Gusev, *Organometallics*, 2009, **28**, 6458–6461.
19 G. Ciancaleoni, N. Scafuri, G. Bistoni, A. Macchioni, F. Tarantelli, D. Zuccaccia and L. Belpassi, *Inorg. Chem.*, 2014, **53**, 9907–9916.
20 K. Verlinden, H. Buhl, W. Frank and C. Ganter, *Eur. J. Inorg. Chem.*, 2015, 2416–2425.
21 A. Liske, K. Verlinden, H. Buhl, K. Schaper and C. Ganter, *Organometallics*, 2013, **32**, 5269–5272.
22 H. Clavier and S. P. Nolan, *Chem. Commun.*, 2010, **46**, 841–861.
23 E. A. Carter and W. A. Goddard III, *J. Phys. Chem.*, 1986, **90**, 998–1001.
24 M. Vasiliu, K. C. Edwards, D. Tapu, C. E. Castillo, T. H. Stein, R. Craciun, A. J. I. Arduengo and D. A. Dixon, *J. Phys. Chem. A*, 2022, **126**, 2658–2669.
25 A. Poater, F. Ragone, S. Giudice, C. Costabile, R. Dorta, S. P. Nolan and L. Cavallo, *Organometallics*, 2008, **27**, 2679–2681.

26 M.-J. Cheng and C.-H. Hu, *Chem. Phys. Lett.*, 2001, **349**, 477–482.
27 R. W. Alder, M. E. Blake, L. Chaker, J. N. Harvey, F. Paolini and J. Schütz, *Angew. Chem., Int. Ed.*, 2004, **43**, 5896–5911.
28 D. C. Graham, K. J. Cavell and B. F. Yates, *J. Phys. Org. Chem.*, 2005, **18**, 298–309.
29 L. Nyulászi, T. Veszprémi and A. Forró, *Phys. Chem. Chem. Phys.*, 2000, **2**, 3127–3129.
30 G. Zhang and C. B. Musgrave, *J. Phys. Chem. A*, 2007, **111**, 1554–1561.
31 A. J. Arduengo, H. V. R. Dias, R. L. Harlow and M. Kline, *J. Am. Chem. Soc.*, 1992, **114**, 5530–5534.
32 J. C. Bernhammer, G. Frison and H. V. Huynh, *Chem.–Eur. J.*, 2013, **19**, 12892–12905.
33 A. A. Tukov, A. T. Normand and M. S. Nechaev, *Dalton Trans.*, 2009, 7015–7028.
34 C. A. Tolman, *Chem. Rev.*, 1977, **77**, 313–348.
35 H. V. Huynh, Y. Han, R. Jothibasu and J. A. Yang, *Organometallics*, 2009, **28**, 5395–5404.
36 G. Meng, L. Kakalis, S. P. Nolan and M. Szostak, *Tetrahedron Lett.*, 2019, **60**, 378–381.
37 S. V. C. Vummaleti, D. J. Nelson, A. Poater, A. Gómez-Suárez, D. B. Cordes, A. M. Z. Slawin, S. P. Nolan and L. Cavallo, *Chem. Sci.*, 2015, **6**, 1895–1904.
38 D. Munz, *Organometallics*, 2018, **37**, 275–289.
39 M. Tretiakov, Y. G. Shermolovich, A. P. Singh, P. P. Samuel, H. W. Roesky, B. Niepötter, A. Visscher and D. Stalke, *Dalton Trans.*, 2013, **42**, 12940–12946.
40 S. Roy, K. C. Mondal and H. W. Roesky, *Acc. Chem. Res.*, 2016, **49**, 357–369.
41 S. Kundu, S. Sinhababu, V. Chandrasekhar and H. W. Roesky, *Chem. Sci.*, 2019, **10**, 4727–4741.
42 V. P. W. Böhm and W. A. Herrmann, *Angew. Chem., Int. Ed.*, 2000, **39**, 4036–4038.
43 J. A. Murphy, *J. Org. Chem.*, 2014, **79**, 3731–3746.
44 J. C. Walton, M. M. Brahmi, J. Monot, L. Fensterbank, M. Malacria, D. P. Curran and E. Lacôte, *J. Am. Chem. Soc.*, 2011, **133**, 10312–10321.
45 T. Taniguchi, *Chem. Soc. Rev.*, 2021, **50**, 8995–9021.
46 R. Bertermann, H. Braunschweig, R. D. Dewhurst, C. Hörl, T. Kramer and I. Krummenacher, *Angew. Chem., Int. Ed.*, 2014, **53**, 5453–5457.
47 Y. Wang, B. Quillian, P. Wei, C. S. Wannere, Y. Xie, R. B. King, H. F. Schaefer, P. v. R. Schleyer and G. H. Robinson, *J. Am. Chem. Soc.*, 2007, **129**, 12412–12413.
48 M. W. Schmidt, K. K. Baldridge, J. A. Boatz, S. T. Elbert, M. S. Gordon, J. H. Jensen, S. Koseki, N. Matsunaga, K. A. Nguyen, S. Su, T. L. Windus, M. Dupuis and J. A. Montgomery, *J. Comput. Chem.*, 1993, **14**, 1347–1363.
49 J.-D. Chai and M. Head-Gordon, *Phys. Chem. Chem. Phys.*, 2008, **10**, 6615–6620.
50 L. Goerigk and S. Grimme, *Phys. Chem. Chem. Phys.*, 2011, **13**, 6670–6688.
51 F. Weigend and R. Ahlrichs, *Phys. Chem. Chem. Phys.*, 2005, **7**, 3297–3305.
52 O. V. Dolomanov, L. J. Bourhis, R. J. Gildea, J. A. K. Howard and H. Puschmann, *J. Appl. Crystallogr.*, 2009, **42**, 339–341.
53 E. D. Glendening, J. K. Badenhoop, A. E. Reed, J. E. Carpenter, J. A. Bohmann, C. M. Morales, P. Karafiloglou, C. R. Landis and F. Weinhold, *NBO 7.0*, Theoretical Chemistry Institute, University of Wisconsin, Madison, Wisconsin, USA, 2018.
54 M. J. Frisch, G. W. Trucks, H. B. Schlegel, G. E. Scuseria, M. A. Robb, J. R. Cheeseman, G. Scalmani, V. Barone, G. A. Petersson, H. Nakatsuji, X. Li, M. Caricato, M. Marenich, J. Bloino, B. G. Janesko, R. Gomperts, B. Mennucci, H. P. Hratchian, J. V. Ortiz, A. F. Izmaylov, J. L. Sonnenberg, D. Williams-Young, F. Ding, F. Lipparini, F. Egidi, J. Goings, B. Peng, A. Petrone, T. Henderson, D. Ranasinghe, V. G. Zakrzweski, J. Gao, N. Rega, G. Zheng, W. Liang, M. Hada, M. Ehara, K. Toyota, R. Fukuda, J. Hasegawa, M. Ishida, T. Nakajima, Y. Honda, O. Kitao, H. Nakai, T. Vreven, K. Throssell, J. A. Montgomery Jr, J. E. Peralta, F. Ogliaro, M. J. Bearpark, J. J. Heyd, E. N. Brothers, K. N. Kudin, V. N. Staroverov, T. A. Keith, R. Kobayashi, J. Normand, K. Raghavachari, A. P. Rendell, J. C. Burant, S. S. Iyengar, J. Tomasi, M. Cossi, J. M. Millam, M. Klene, C. Adamo, R. Cammi, J. W. Ochterski, R. L. Martin, K. Morokuma, O. Farkas, J. B. Foresman and D. J. Fox, *Gaussian 16 (version Revision C.01)*, Gaussian, Inc., Wallingford, CT, USA, 2019.
55 F. Neese, F. Wennmohs, U. Becker and C. Riplinger, *J. Chem. Phys.*, 2020, **152**, 224108.
56 C. van Wüllen, *J. Chem. Phys.*, 1998, **109**, 392–399.
57 J. P. Perdew, K. Burke and M. Ernzerhof, *Phys. Rev. Lett.*, 1996, **77**, 3865–3868.
58 J. D. Rolfes, F. Neese and D. A. Pantazis, *J. Comput. Chem.*, 2020, **41**, 1842–1849.